A study of the BrO and BrO_2 radicals with vacuum ultraviolet photoelectron spectroscopy

J. M. Dyke,[a] S. D. Gamblin,[b] N. Hooper, E. P. F. Lee,[c] and A. Morris
Department of Chemistry, University of Southampton, Southampton SO17 1BJ, United Kingdom

D. K. W. Mok and F. T. Chau
Department of Applied Biology and Chemical Technology, Hong Kong Polytechnic University, Hung Hom, Hong Kong, China

(Received 14 September 1999; accepted 12 January 2000)

The BrO radical, prepared by the $Br+O_3$ reaction, has been investigated by ultraviolet photoelectron spectroscopy. Two vibrationally resolved bands were observed corresponding to the ionizations $BrO^+(X\,^3\Sigma^-)\leftarrow BrO(X\,^2\Pi)$ and $BrO^+(a\,^1\Delta)\leftarrow BrO(X\,^2\Pi)$. These assignments are supported by the results of complete active space self-consistent field/multireference configuration interaction (CASSCF/MRCI) calculations performed as part of this work. The adiabatic ionization energies of these bands were measured as (10.46 ± 0.02) and (11.21 ± 0.02)eV, respectively. Measurement of the vibrational separations in these bands led to estimates of the vibrational constants in the ionic states of $(840\pm30)\ cm^{-1}$ and $(880\pm30)\ cm^{-1}$, and Franck–Condon simulations of the vibrational envelopes gave values of the ionic state bond lengths of (1.635 ± 0.005) and (1.641 ± 0.005) Å for the $X\,^3\Sigma^-$ and $a\,^1\Delta$ states of BrO^+, respectively. The $O+Br_2$ reaction was found to give a band at (10.26 ± 0.02) eV associated with a reaction product. Comparison of the results obtained for the $Br+O_3$ reaction showed that it could not be assigned to ionization of BrO. Calculations of the first adiabatic ionization energies and Franck–Condon simulations of the vibrational envelopes of the first photoelectron bands of BrO_2 and Br_2O and their isomers demonstrated that this band corresponds to the first ionization of OBrO, the $BrO_2^+(X\,^1A_1)\leftarrow BrO_2(X\,^2B_1)$ ionization. Franck–Condon simulations were performed with the experimental geometry of $BrO_2(\tilde{X}\,^2B_1)$ but with different cationic state geometries. The simulated envelope which most closely matched the experimental envelope gave geometrical parameters of $r_e=1.6135$ Å and $\angle OBrO=117.5°$ for the ionic state. © *2000 American Institute of Physics.* [S0021-9606(00)00214-2]

I. INTRODUCTION

The importance of bromine in the earth's atmosphere, particularly in reactions that lead to the loss of ozone, is now widely recognized.[1–3] Although less abundant than chlorine, it has a greater potential to destroy stratospheric ozone since catalytic cycles involving BrO are more efficient than those involving ClO.

An understanding of the consequences of bromine–oxidant reactions requires a knowledge of the properties of the molecules involved, such as their ionization energies, electron affinities, equilibrium structures, and vibrational constants. These quantities are valuable in thermochemical cycles used to determine the heats of formation of bromine oxides, notably BrO, BrO_2, and Br_2O.

The BrO radical has a $^2\Pi_{3/2}$ ground state. It has been investigated experimentally by microwave,[4] infrared,[5] and cavity ring down spectroscopy,[6] as well as with electronic structure calculations.[7–9] Similar studies have also been made on Br_2O and BrO_2.[10–16]

The ionization energy of BrO was first reported in 1978[17] when ultraviolet (UV) photoelectron spectroscopy was used to study the $O+Br_2$ reaction. A sharp band associated with a reaction product, with the adiabatic component equal to the vertical component at 10.29 eV, was assigned to the first ionization of BrO, the $BrO^+(X\,^3\Sigma^-)\leftarrow BrO(X\,^2\Pi)$ ionization. Much more recently, a photoionization mass spectrometric (PIMS) study of BrO, produced from the $O+Br_2$ reaction, determined the first adiabatic ionization energy of BrO as (10.46 ± 0.02) eV.[18]

Of the values for the first ionization energy of BrO derived from molecular orbital calculations,[7,8] the most recent and reliable value is (10.455 ± 0.035) eV,[7] obtained by performing CCSD(T) calculations with large atomic natural orbital basis sets and extrapolating the result to the one-particle basis set limit. For the triatomic bromine oxides, Br_2O and BrO_2, the first adiabatic ionization energy (AIE) of Br_2O has been measured as (10.26 ± 0.01) eV by PIMS[19] and the first AIE of BrO_2 has been calculated at the CCSD(T) level as (10.16 ± 0.13) eV.[20] BrO_2 is also known as a secondary product of the $O+Br_2$ reaction,[21] and Br_2O has been prepared by passing bromine over solid mercuric oxide.[11]

The aim of this work was to explain the reason for the discrepancy between the early photoelectron spectroscopy (PES) value for the first AIE of BrO of (10.29 ± 0.01) eV[17]

[a]Author to whom correspondence should be addressed.
[b]Current address: CPES, University of Sussex, Falmer, Brighton BN1 9QJ, United Kingdom.
[c]Also at Department of Applied Biology and Chemical Technology, Hong Kong Polytechnic University, Hung Hom, Hong Kong, China.

and the more recent PIMS value of (10.46 ± 0.02) eV.[18] For this purpose, the reactions $Br+O_3$ and $O+Br_2$ were studied at different reaction times by ultraviolet (UV) photoelectron spectroscopy.

II. EXPERIMENT

HeI (21.22 eV) photoelectron spectra were recorded for the $Br+O_3$ and $O+Br_2$ reactions using a single detector photoelectron spectrometer specifically designed to study short-lived species in the gas phase.[22] Under typical operating conditions, the resolution as measured from the full width at half maximum (FWHM) of the $Ar^+(^2P_{3/2})\leftarrow Ar(^1S_0)(3p)^{-1}$ photoelectron band was approximately 30 meV. Spectra were obtained by linearly sweeping the pass energy of an electrostatic hemispherical analyzer. At 5.5 eV pass energy, the resolution was approximately 30 meV, and at 11.0 eV pass energy the resolution was approximately 60 meV. Spectra were calibrated using the known ionization energies of the reactants and stable product species, notably O, Br, and O_2, as well as methyl iodide which was added to the ionization region.

In practice, it was found that a higher partial pressure of BrO could be produced from the $Br+O_3$ reaction than from $O+Br_2$. This was because although the rate constant of the $Br+O_3$ primary reaction (k_1) is an order of magnitude less than that of the $O+Br_2$ reaction (k_2), the secondary reaction which removes BrO associated with reaction (1) [reaction (3)] is much slower than the secondary reaction which removes BrO associated with reaction (2) [reaction (4)].

The rate constant of these reactions, at 298 K, is[23]

$$Br+O_3\rightarrow BrO+O_2,$$
$$k_1=(1.2\pm0.2)\times10^{-12}\,cm^3\,mol^{-1}\,s^{-1}, \quad (1)$$

$$O+Br_2\rightarrow BrO+Br, \quad k_2=(1.2\pm0.4)\times10^{-11}\,cm^3\,mol^{-1}\,s^{-1}, \quad (2)$$

$$BrO+O_3\rightarrow Br+2O_2, \quad k_3<2\times10^{-17}\,cm^3\,mol^{-1}\,s^{-1}, \quad (3)$$

$$BrO+O\rightarrow Br+O_2, \quad k_4=4.1\times10^{-11}\,cm^3\,mol^{-1}\,s^{-1}. \quad (4)$$

To study the $Br+O_3$ reaction, Br atoms were produced by passing a flowing mixture of $SiBr_4$ and argon through a microwave discharge (2.45 GHz). Preliminary experiments showed that a microwave discharge of $SiBr_4$ did not produce any photoelectron signals other than those seen in a photoelectron spectrum of discharged Br_2. Discharged $SiBr_4$ was, however, preferred as a source of Br atoms since good yields of Br atoms were obtained and problems associated with contamination of the ionization region and signal stability over a long period are considerably less than those encountered when using Br_2.[24] Ozone was produced by a 10 kV silent discharge of flowing molecular oxygen and was collected by adsorbing it onto silica gel contained within a U-tube cooled to 195 K by use of a dry ice/acetone slush bath.[25] After several hours of ozone production, the U-tube was removed from the ozonizer and attached to the spectrometer, where the ozone was allowed to desorb by slowly raising the tube out of the cooling bath. Virtually pure ozone was admitted to the spectrometer through a thin [3 mm outer diameter (o.d.)] inlet tube positioned down the center of the tube used to carry the Br/Ar mixture. The inner tube could be moved with respect to the outer tube, whilst maintaining the low pressure in the inlet system, so that the position at which O_3 was introduced into the Br atom flow could be altered in the range 0–30 cm above the photon beam. This feature of the inlet system enabled the production of BrO and the secondary products of the $Br+O_3$ reaction to be studied as a function of mixing distance. This mixing distance range corresponds approximately to reaction times in the range 0–15 ms. All internal surfaces of the glass inlet system were carefully pretreated with phosphoric acid to minimize surface catalyzed recombination reactions. Experiments conducted in the absence of ozone were able to show that the Br atom yield was unaffected by the position of the moveable inlet tube.

A similar inlet system was used to study the products of the $O+Br_2$ reaction as a function of mixing distance above the photon beam. In these experiments O atoms were produced in the outer inlet tube by passing a flowing mixture of O_2 and argon through a microwave discharge and Br_2 was introduced to the oxygen flow above the photon beam via the moveable inner tube. All the internal surfaces of this glass inlet system were carefully pretreated with boric acid.

III. COMPUTATIONAL DETAILS

Ab initio molecular orbital calculations were carried out on BrO, and a number of isomers of Br_2O and OBrO, as well as their low-lying cationic states. Most of the calculations were carried out using the GAUSSIAN 94 and 98 suites of programs,[26] although some calculations were performed with MOLPRO.[27] All quantum chemical calculations presented in this work were performed with the cluster of DEC 8400 machines at the Rutherford-Appleton Laboratory, EPSRC, United Kingdom.

In order to aid assignment of bands observed in the $Br+O_3$ and $O+Br_2$ reactions associated with reaction intermediates, adiabatic ionization energies (AIEs) and vertical ionization energies (VIEs) and Franck–Condon factors were computed for photoelectron bands of BrO, BrO_2, and Br_2O and other isomers. Details of the calculations performed for each molecule and the results obtained will be presented later in Sec. IV.

IV. RESULTS AND DISCUSSION

A. The $Br+O_3$ reaction studied by PES

A photoelectron spectrum recorded for O_3, mixed with $SiBr_4$ and Ar at a distance of 15 cm above the photon beam, is shown in Fig. 1(a). The ozone sample is virtually free from oxygen and hence the spectrum shows only a very small contribution from O_2. The first three bands of O_3 can be seen in the ionization energy range 12.5–14.0 eV[25] and the first four bands of $SiBr_4$ are observed in the range 10.5–12.5 eV.[28]

Figure 1(b) shows the photoelectron spectrum recorded for the same gas sample but with the $SiBr_4$/Ar mixture being passed through a microwave discharge before it is mixed with O_3 15 cm above the photon beam. There is no undisso-

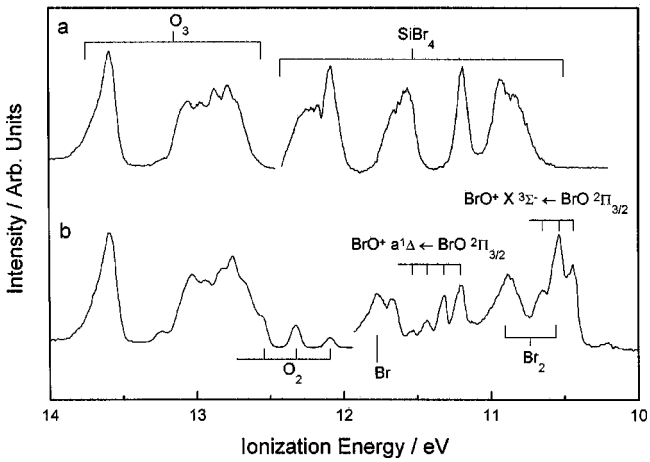

FIG. 1. Figure 1(b) shows the HeI photoelectron spectrum obtained for the $Br+O_3$ reaction at a mixing distance of 15 cm above the photon beam. Br atoms were prepared by microwave discharge of a $SiBr_4$/Ar mixture. Figure 1(a) was obtained for the same reaction mixture, but with the microwave discharge turned off. The intensity of the third band of ozone in these spectra is approximately 2500 counts s^{-1}. The count rate scale used to record the 10.0–11.9 eV ionization energy range was ten times lower than that used to record the 11.9–14.0 eV region.

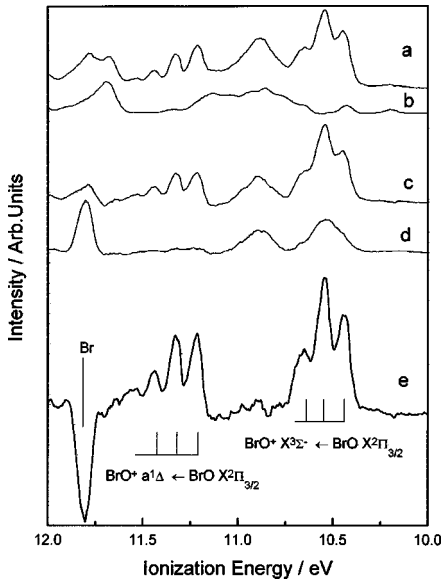

FIG. 2. (a) 10.0–14.0 eV ionization energy region of the HeI photoelectron spectrum recorded for the $Br+O_3$ reaction at a mixing distance of 15 cm above the photon beam. (b) HeI_β signals arising from O_3 and O_2 in the 10.0–14.0 eV ionization energy region. (c) The photoelectron spectrum obtained by subtracting 2(b) from 2(a). (d) HeI photoelectron spectrum recorded in the 10.0–14.0 eV ionization energy region for discharged $SiBr_4$/Ar showing bands arising from Br_2 and Br. (e) HeI photoelectron spectrum obtained by subtracting 2(d) from 2(c) (see text for further details).

ciated $SiBr_4$ in this spectrum and the presence of Br atoms is confirmed by a band at 11.81 eV corresponding to the ionization $Br^+(^3P_2) \leftarrow Br(^2P_{3/2})$.[24,29] The first band of oxygen is also clearly seen in this figure, indicating that the reaction $Br+O_3 \rightarrow BrO+O_2$ is occurring. For reaction products to be observed, it was found that $[O_3]$ must be in considerable excess relative to [Br] and as a result signals arising from HeI_β (23.09 eV) ionization of O_3 were present in the 10.0–12.0 eV ionization energy region of the $HeI\alpha$ spectrum. This region was further complicated by signals arising from Br_2, formed by recombination of Br atoms. Ionization to the second spin-orbit component of the ground state of Br_2^+ gives a band at 10.91 eV. Ionization to the first spin-orbit component of the ground state of Br_2^+ gives a band at 10.55 eV, but this is overlapped by at least three additional features associated with a short-lived reaction intermediate. Another unidentified structured photoelectron band associated with a reaction intermediate is observed in Fig. 1(b) at approximately 11.2 eV ionization energy. These two bands, which have been assigned to BrO on the basis of evidence which will be presented later, have AIEs of (10.46 ± 0.02) and $(11.21 \pm 0.02\,\text{eV})$. They showed the same intensity ratio under all experimental conditions of (1.3 ± 0.1), corrected for analyzer transmission, in reasonable agreement with the 3:2 intensity ratio expected for the lowest energy ionizations of BrO, $BrO^+(X\,^3\Sigma^-) \leftarrow BrO(X\,^2\Pi)$ and $BrO^+(a\,^1\Delta) \leftarrow BrO(X\,^2\Pi)$.

Figure 2(a) reproduces the 10.0–12.0 eV region of the $Br+O_3$ spectrum recorded at a mixing distance of 15 cm [Fig. 1(b)]. Beneath this, in Fig. 2(b), is an estimate of the signals arising from HeI_β ionization of O_3 and O_2 in Fig. 2(a). This was obtained by taking the 12.0–14.0 eV ionization energy region of the spectrum shown in Fig. 1(b), moving it to lower ionization energy on the HeI_α scale by 1.87 eV (the $HeI_\alpha - HeI_\beta$ energy separation), and adjusting the intensity such that the intensity of the O_2 first band features and the O_3 third band match those observed in the 10.0–12.0 eV region as HeI_β signals. Figure 2(c) shows the result of subtracting the HeI_β estimate [Fig. 2(b)] from the experimental spectrum [Fig. 2(a)]. The same procedure was adopted for the spectrum recorded at a mixing distance of 0 cm and this is shown, after subtraction of the HeI_β contributions, in Fig. 2(d). At this mixing distance, no reaction has occurred and the two bands assigned to BrO are absent. Also, the Br atom band at 11.81 eV in Fig. 2(d) is, as expected, considerably more intense at this mixing distance than that observed in the spectrum recorded at a mixing distance of 15 cm [Fig. 2(c)].

Having obtained two spectra [Figs. 2(c) and 2(d)] which are wholly attributable to $HeI\alpha$ signals, the Br_2 contribution to the spectrum recorded at a mixing distance of 15 cm [Fig. 2(c)] was removed by subtracting the spectrum recorded at 0 cm [Fig. 2(d)]. The result is the spectrum shown in Fig. 2(e), in which the positive signals are those arising from reaction products and the reactants (only Br atoms, in this region of the spectrum) appear as negative features. It should be noted that this subtraction procedure has not introduced any structure which could not be observed in the original spectrum recorded for the $Br+O_3$ reaction.

The adiabatic ionization energy of the first BrO photoelectron band, assigned to the $BrO^+(X\,^3\Sigma^-) \leftarrow BrO(X\,^2\Pi)$ ionization, is measured as $(10.46 \pm 0.02\,\text{eV})$ in very good agreement with the recent PIMS value of (10.46 ± 0.02) eV.[18] Three regularly spaced vibrational components are observed. Measurement of the vibrational spacings led to an estimate of the vibrational constant, ω_e, in the ionic state of $(840 \pm 30)\ \text{cm}^{-1}$. The second photoelectron band of BrO, corresponding to the ionization $BrO^+(a\,^1\Delta) \leftarrow BrO(X\,^2\Pi)$,

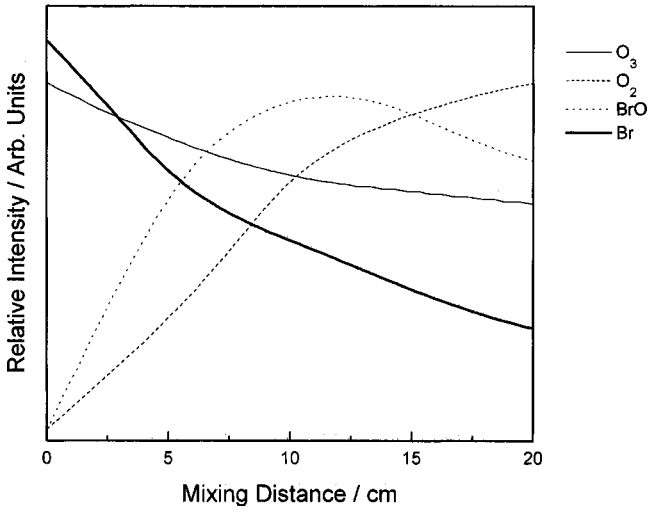

FIG. 3. Variation of the intensity of the photoelectron bands of O_3, O_2, BrO, and Br as a function of mixing distance above the photon beam for the $Br+O_3$ reaction, recorded at constant reagent partial pressure. 1 cm mixing distance is approximately equal to 0.5 ms reaction time.

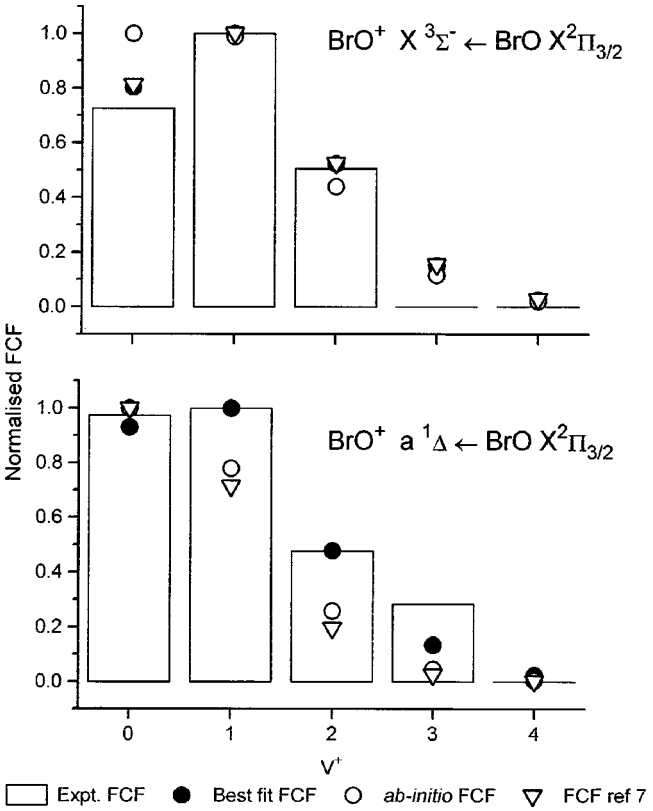

FIG. 4. Comparison of the experimental vibrational component intensities in the first two photoelectron bands of BrO with the best-fit vibrational envelope, obtained by variation of the equilibrium bond length in the ionic state. Also, shown in this diagram are the Franck–Condon factors obtained from CASSCF/MRCI calculations performed as part of this work and the CCSD(T) calculations of Ref. 7. See text for further details.

is observed at an AIE of $(11.21\pm0.02\,\text{eV})$. Three vibrational components were observed in this band with the possibility of a fourth. Measurement of the vibrational spacings led to an estimate of the vibrational constant, ω_e, in the ionic state of $(880\pm30)\ \text{cm}^{-1}$.

The ground-state electronic configuration of BrO is known to be[17]

$$\cdots 8\sigma^2 9\sigma^2 10\sigma^2 4\pi^4 5\pi^3.$$

The first three photoelectron bands of BrO are expected to arise from the $(5\pi)^{-1}$ ionization, which gives rise to the $X\,^3\Sigma^-$, $a\,^1\Delta$, and $b\,^1\Sigma^+$ ionic states. As the 5π molecular orbital is antibonding in character, the vibrational constants, ω_e, in the first and second photoelectron bands are expected to be greater than the vibrational constant, ω_e, in the $X\,^2\Pi$ state of BrO ($725.7\ \text{cm}^{-1}$),[5] as is the case. Also, as the spin-orbit splitting in BrO $X\,^2\Pi$ is $815\ \text{cm}^{-1}$,[30] the population of the $X\,^2\Pi_{1/2}$ state relative to that of the $X\,^2\Pi_{3/2}$ state is expected to be very small at room temperature and as a result the observed bands are expected to arise only from ionization of the $X\,^2\Pi_{3/2}$ state. Unfortunately, the third band of BrO, corresponding to the $BrO^+(b\,^1\Sigma^+)\leftarrow BrO(X\,^2\Pi)$ ionization, could not be observed because of overlap with more intense bands in the 11.6–12.1 eV region, notably bands of Br atoms, O_2, and the third band of O_3 recorded with HeI_β radiation. Photoionization of BrO $X\,^2\Pi_{3/2}$ with a Boltmann vibrational distribution at room temperature is consistent with the spectra obtained. The $Br+O_3$ reaction [reaction (1)] is exothemic by 1.4 eV. The BrO produced is almost certainly produced vibrationally excited, but no evidence for this was obtained from the experimental spectra. It appears that BrO is collisionally vibrationally deactivated between the point of production and photoionization.

Photoelectron spectra were recorded at constant reagent partial pressures at a range of mixing distances in the region 0–30 cm. The relative intensities of all reactant and product bands were measured at each mixing distance, from difference spectra obtained by the procedure outlined above, and these are plotted in Fig. 3. As can be seen from this figure, the relative concentration of the reactants decreases with mixing distance while the stable product (O_2) increases steadily. The mixing distance profiles of the two BrO bands closely resemble each other, supporting their assignment to ionization of the same neutral species. The short-lived nature of the molecule associated with these bands is confirmed by the way their intensities initially increase for short mixing distances (<10 cm) and then decrease at mixing distances greater than 10 cm, corresponding to reaction times greater than 5 ms.

Using the procedure outlined previously,[31] the relative intensity of the vibrational components in the first two bands of BrO was used to estimate the change in equilibrium bond length on ionization. The method involved assuming that each state was well represented by a Morse potential, which is determined by values of ω_e, $\omega_e x_e$, and r_e. For the $X\,^2\Pi_{3/2}$ state of BrO these values are well established.[4,5,30] However, for each ionic state ω_e was determined from the experimental vibrational spacings. For each ionization, Franck–Condon factors were computed for a range of possible ionic r_e values and the computed vibrational profiles were compared to the experimental envelopes by means of a least-squares procedure. Using this method, the values of r_e which give the best fit to the experimental envelopes were

TABLE I. Computed and experimental spectroscopic constants of BrO and BrO^+.

Parameter state	ω_e /cm^{-1}	$\omega_e x_e$ /cm^{-1}	r_e /Å	
BrO $X\,^2\Pi$	725.7	4.74	1.7207	Ref. 5
	715.1	5.43	1.728	CASSCF/MRCI calcs; this work
	728	···	1.725	Ref. 7: RCCSD(T)/ANO4
BrO^+ $X\,^3\Sigma^-$	840±30	···	1.635±0.005	This work; see text
	875	5.03	1.651	CASSCF/MRCI calcs; this work
	854	···	1.640	Ref. 7: RCCSD(T)/ANO4
BrO^+ $a\,^1\Delta$	880±30	···	1.641±0.005	This work; see text
	850	5.99	1.659	CASSCF/MRCI calcs; this work
	804	5.99	1.659	Ref. 7: CCSD(T)/6-311+G(3df)
BrO^+ $b\,^1\Sigma^+$	794.6	6.66	1.673	CASSCF/MRCI calcs; this work

(1.635±0.005) and (1.641±0.005) Å for the $X\,^3\Sigma^-$ and $a\,^1\Delta$ states of BrO^+, respectively. The Franck–Condon factors computed with these bond lengths are compared with the experimental relative vibrational intensities in Fig. 4.

The values obtained in this work for the spectroscopic constants r_e and ω_e for the $BrO^+(X\,^3\Sigma^-)$ state [(840 ±30) cm^{-1} and (1.635±0.005) Å] compare reasonably favorably with the corresponding values derived from CCSD(T) calculations[7] (854 cm^{-1} and 1.640 Å).

B. *Ab initio* calculations on BrO

In the present investigation, CASSCF/MRCI potential curves were computed with the cc-pVQZ basis set (without g functions) for the $X\,^2\Pi$ state of BrO and the $X\,^3\Sigma^-$, $a\,^1\Delta$, and $b\,^1\Sigma^+$ states of BrO^+. These potential curves were used primarily to generate vibrational wave functions and then Franck–Condon factors for the ionization processes $BrO^+(X\,^3\Sigma^-)\leftarrow BrO(X\,^2\Pi)$ and $BrO^+(a\,^1\Delta)\leftarrow BrO(X\,^2\Pi)$. It has already been noted that the lowest energy electronic configuration in the cation has the open-shell π^2 configuration, which gives rise to the $^3\Sigma^-$, $^1\Delta$, and $^1\Sigma^+$ states. Whilst the two singlet states are not described correctly by single-configuration [restricted Hartree–Fock (RHF) or unrestricted Hartree–Fock (UHF)] wave functions, as used in the CCSD(T) calculations of Francisco *et al.*,[7] the CASSCF and MRCI methods employed in this work give the correct wave functions for all the states investigated and do not suffer from spin contamination. The CASSCF/MRCI calculations were carried out using the MOLPRO suite of programs.[27] Spectroscopic constants (r_e, ω_e, and $\omega_e x_e$) were derived from the potential curves using a program (LEVEL),[32] which solves the radial Schrödinger equation with a given potential curve to obtain rotational and vibrational eigenvalues. The spectroscopic constants obtained, as well as the adiabatic ionization energies, are shown in Tables I and II. In each case, the computed vibrational constants are, within experimental error, in agreement with the experimental values. The computed equilibrium bond lengths are slightly longer (by ≈0.015 Å) than the experimental values. The computed AIEs are both lower than the experimental values by ≈0.25 eV, although the separation between the calculated values (0.75 eV) agrees well with the experimental separation [(0.75±0.02) eV]. The spectroscopic constants derived from the CASSCF/MRCI calculations performed in this work have been used to define Morse potentials for the states involved and then to compute the vibrational envelopes for the first two photoelectron bands of BrO. Using the same approach, Franck–Condon calculations have also been performed using the results of the CCSD(T) calculations of Ref. 7. As can be seen from Fig. 4, the results obtained with both the CASSCF/MRCI calculations of this work and the CCSD(T) calculations of Ref. 7 show good agreement with the experimental envelope.

C. The O+Br_2 reaction studied by PES

Figure 5(a) shows a photoelectron spectrum recorded for a mixture of O_2 and Br_2 under conditions where the Br_2 was introduced into an O_2 flow 10 cm above the photon beam. The only significant signals in this spectrum are those associated with ionization of $O_2(X\,^3\Sigma_g^-)$ in the 12.0–13.0 eV region and with ionization of Br_2 in the 10.5–11.0 eV region. Figure 5(b) shows the spectrum recorded for the same mix-

TABLE II. Computed and experimental adiabatic ionization energies (AIEs)/eV of BrO.

Ionization	AIE Experimental this work	AIE CASSCF/MRCI this work	AIE CCSD(T)/ANO Ref. 7
$BrO^+(X\,^3\Sigma^-)\leftarrow BrO(X\,^2\Pi)$	10.46±0.02[a]	10.18[b]	10.455±0.035
$BrO^+(a\,^1\Delta)\leftarrow BrO(X\,^2\Pi)$	11.21±0.02	10.93	11.42
$BrO^+(b\,^1\Sigma^+)\leftarrow BrO(X\,^2\Pi)$	···	11.46	···

[a]In Ref. 18, the first AIE of BrO, prepared from the O+Br_2 reaction, has been measured by PIMS as (10.46 ±0.02) eV.

[b]AIE obtained at RCCSD(T)/cc-PVQZ(s, p, d, f, g) level with CASSCF/MRCI computed geometries is 10.34 eV.

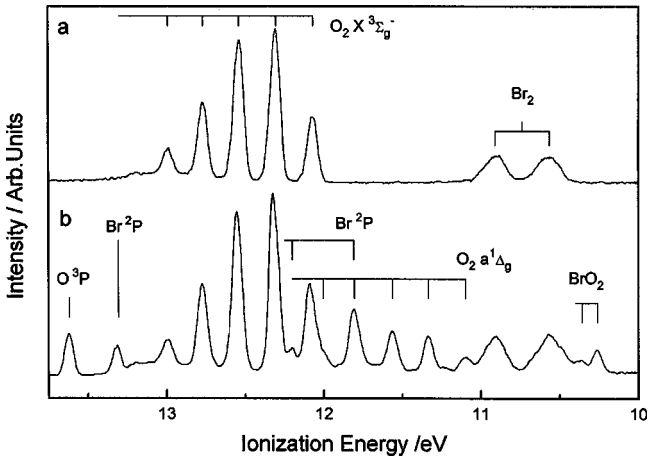

FIG. 5. HeI photoelectron spectra recorded in the 10.0–13.8 eV ionization energy range for Br_2 reacted with discharged oxygen at a mixing distance of 10 cm above the photon beam. Figures 5(b) and 5(a) were recorded with the oxygen discharge on and off, respectively. The count-rate obtained on the first two bands of Br_2 in the 10.5–11.0 eV ionization energy region is ≈600 coounts s^{-1}.

ture with the O_2 discharged before it is mixed with the Br_2. The microwave discharge produces a significant amount of $O_2(a\,^1\Delta_g)$ and oxygen atoms, $O(^3P)$. Signals arising from ionization of these discharge products can be clearly seen in the 11.0–12.0 eV region [corresponding to $O_2^+(X\,^2\Pi_g) \leftarrow O_2(a\,^1\Delta_g)$] and at 13.61 eV [corresponding to $O^+(^4S) \leftarrow O(^3P)$]. Experiments performed for discharged oxygen alone demonstrated that the intensity of the O atom signal at 13.61 eV was approximately equal to the most intense O_2 signal, the $O_2^+(X\,^2\Pi_g)$, $v^+=1 \leftarrow O_2(X\,^3\Sigma_g^-)$, $v''=0$ feature. The intensity of the O atom signal at 13.61 eV decreased as the O_2/O mixture is reacted with Br_2 and this decrease is accompanied by the appearance of Br atom bands. In addition to these features, the spectrum recorded for Br_2 reacted with discharged oxygen [Fig. 5(b)] shows two features which were part of a short vibrational progression with an adiabatic ionization energy of (10.26 ± 0.02) eV. This band was shown to arise from the $O+Br_2$ reaction by performing experiments in which the O atoms, but not the $O_2(a\,^1\Delta_g)$ from the O_2 discharge, were deactivated by using a glass-wool plug placed in the O_2 discharge sidearm. Spectra recorded under these conditions showed no evidence of reaction and the band at 10.26 eV was not seen.

The spectrum presented in Fig. 5(b), as well as the position and envelope of the band at 10.26 eV, agrees very well with that published in the original $O+Br_2$ PES study.[17] However, based on the results obtained from the $Br+O_3$ reaction in this work, which placed the first AIE of BrO at (10.46 ± 0.02) eV, and the supporting theoretical and PIMS evidence,[18] the assignment of the band at 10.26 eV to ionization of BrO made in the earlier study[17] is clearly incorrect.

In order to obtain the vibrational envelope of the band at 10.26 eV in the absence of Br_2 and $O_2(a\,^1\Delta_g)$ features, the signals due to Br_2 and $O_2(a\,^1\Delta_g)$ were subtracted off. Figure 6(a) is a reproduction of the 10.0–11.5 eV region of the $O+Br_2$ spectrum shown in Fig. 5(b). Figure 6(b) shows a spectrum of discharged O_2 recorded under approximately the same experimental conditions as Fig. 6(a). The first two vibrational components of the $O_2(a\,^1\Delta_g)$ photoelectron band, $O_2^+(X\,^2\Pi_g) \leftarrow O_2(a\,^1\Delta_g)$, are clearly seen in the 11.0–11.5 eV region and the second of these is used to normalize this spectrum to the $O_2(a\,^1\Delta_g)$ band in the $O+Br_2$ spectrum. Much weaker signals due to HeI_β ionization of $O_2(X\,^3\Sigma_g^-)$ are present at lower apparent ionization energy. A photoelectron spectrum of the first band of Br_2 is shown in Fig. 6(c). This spectrum has been normalized so that the intensity of the second spin-orbit component is the same as that of the corresponding band in the $O+Br_2$ spectrum [Fig. 6(a)]. The result of subtracting the Br_2 and the discharged O_2 spectra from the $O+Br_2$ spectrum is shown in Fig. 6(d). As can be seen, the vibrational envelope of the first band of the reaction product at 10.26 eV only shows two components with the vertical the same as the adiabatic. The two components were separated by (820 ± 30) cm^{-1} and they maintained the same intensity ratio as the experimental conditions were changed. No evidence was obtained for another band associated with this feature. Very weak features were, however, observed at 10.46 and 11.21 eV, which were the BrO bands, observed with more intensity in the $Br+O_3$ reaction.

The relative intensity of the main observable features in the $O+Br_2$ reaction were monitored as a function of mixing distance at constant reagent partial pressure and the results obtained are summarized in Fig. 7. As expected, the O atoms decrease with increasing mixing distance. The 10.26 eV band increases to ≈5.0 cm mixing distance and then decreases, demonstrating that it is associated with a reaction product of limited lifetime under the conditions used.

D. *Ab initio* calculations on BrO_2 and Br_2O

As the band at 10.26 eV observed from the $O+Br_2$ reaction cannot be assigned to BrO, it was clear that it must be associated with a secondary reaction product. As Br_2O has a first AIE of (10.26 ± 0.01) eV measured by PIMS[19] and BrO_2 is a known secondary product of the $O+Br_2$ reaction[21] with a computed first AIE at the CCSD(T) level of (10.16 ± 0.13) eV,[20] these were the two major candidates considered for assignment of the 10.26 eV band. In fact, the band at 10.26 eV could be unambiguously assigned to ionization of BrO_2 with a C_{2v} structure (see later).

Ab initio calculations were performed for Br_2O and BrO_2 in order to compute their first AIEs. Other than comparing the computed AIEs and the harmonic vibrational frequencies of the cation with the observed values, spectral simulations were also carried out for comparison with the observed vibrational envelope, in order to obtain an unambiguous assignment for the observed photoelectron band at 10.26 eV. For both BrO_2 and Br_2O, the Cartesian Franck–Condon Factor (CART-FCF) program was employed, which is based on the harmonic oscillator model and includes Duschinsky rotation. The details of the Franck–Condon method employed (the IFCA method) have been described previously.[33]

1. $OBrO(C_{2v})$ and its cation

In this work, minimum energy geometries and harmonic frequencies were computed at several levels of theory with different standard basis sets for the ground states of BrO_2

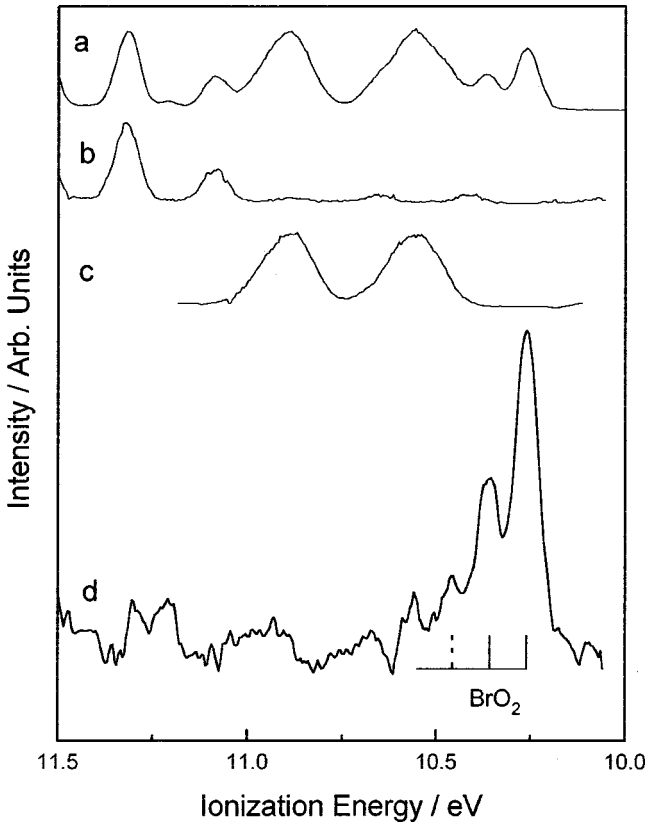

FIG. 6. (a) HeI photoelectron spectrum recorded in the 10.0–11.5 eV region for the $O+Br_2$ reaction at 10 cm mixing distance above the photon beam. (b) A HeI photoelectron spectrum of discharged oxygen recorded under the same experimental conditions used to obtain Fig. 6(a). (c) A HeI photoelectron spectrum of Br_2 recorded in the ionization energy region 10.0–11.5 eV. This spectrum has been normalized so that the Br_2 band intensity is the same as that in Fig. 6(a). (d) The result of subtracting Figs. 6(b) and 6(c) from Fig. 6(a).

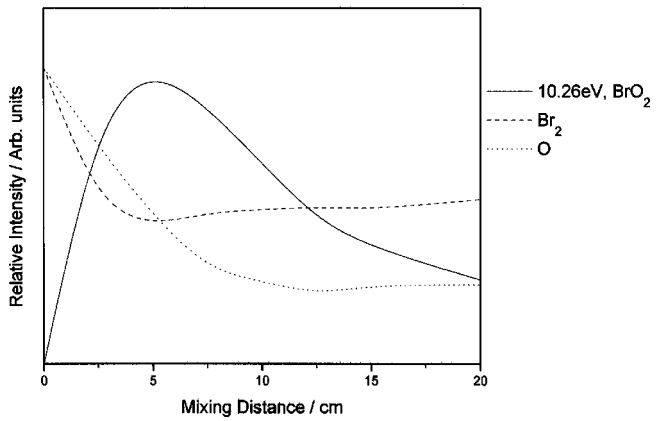

FIG. 7. Variation of the intensity of the photoelectron bands O, Br_2, and BrO_2 as a function of mixing distance above the photon beam for the reaction $O+Br_2$, recorded at constant reagent partial pressure. 1 cm mixing distance is approximately equal to 0.5 ms reaction time.

and BrO_2^+. An augmented effective core potential (ECP) basis set, lan12 $dz+2d$ (the lan12 ECP with the standard double-zeta valence basis,[34] augmented with one set of diffuse *sp* and two sets of *d* Gaussian functions) was also used for Br [together with the 6-31+G(2*d*) basis set for O]; this basis set has been used in calculations for BBr_2 and its cation and was found to be satisfactory.[35] Single geometry energy calculations at a higher level and/or with a larger basis set, including the G2 method,[36] were also performed to obtain improved AIEs.

When these calculations on BrO_2 and BrO_2^+ were started, it was noted that the first AIE of BrO_2 had been calculated at the CCSD(T)/6-311+G(3*df*)//CCSD(T)/6-311G(2*df*) level as (10.16 ± 0.13) eV and the symmetric stretching frequency of the cation had been computed as 822 cm^{-1} at the CCSD(T)/TZ2P level.[20] Both the computed AIE and the vibrational frequency match reasonably well with the corresponding values obtained from the HeI $O+Br_2$ photoelectron spectrum for the 10.26 eV band. However, the HeI photoelectron spectrum of OClO has been reported[37] and the first band has a vibrational envelope which differs significantly from what is observed for the 10.26 eV band seen in the $O+Br_2$ reaction.

2. BrO_2 optimized geometries, computed harmonic vibrational frequencies, and ionization energies

The results obtained for BrO_2 and BrO_2^+ are summarized in Tables III–VII, where they are compared with the most recent computed values in the literature [experimental values are available only for the neutral ground state; see Table III].

TABLE III. $BrO_2(\tilde{X}\,^2B_1)$ computed minimum energy geometries and harmonic vibrational frequencies.

Method	r_e/A	OBrO/deg	Sym. str.	Sym. bend	Asym. str	Ref.
MP2/6-31G*	1.672	116.6	874	320	894	this work
QCISD/6-31G*	1.684	115.4	770	308	845	this work
QCISD/6-311G(2*d*)	1.652	114.8	803	323	876	this work
QCISD/6-311+G(3*df*)	1.634	113.7	917	337	852	this work
CCSD(T)/TZ2P	1.660	114.8	797	317	845	20
CCSD(T)/6-311G(2*df*)	1.644	114.8	⋯	⋯	⋯	20
CCSD(T)/6-311+G(3*df*)	1.646	114.3	⋯	⋯	⋯	this work
CAS/MRCI/ECP, pVQZ	1.646	114.7	806.5	319.5	869.4	43
QCISD(T)/ECT+(2*df*)	1.659	115.2	850	308	781	15
Expt.	1.644	114.3	811.6	320.2	865.6	2
Expt.	1.649	114.4	795.7	317.0	845.2	15
Expt.	1.649	114.8	799.4	317.5	848.6	20

TABLE IV. $BrO_2^+(\tilde{X}\,^1A_1)$ computed minimum energy geometries and harmonic vibrational frequencies.

Method	r_e/A	OBrO/deg	Sym. str.	Sym. bend	Asym. str	Ref.
MP2/6-31G*	1.656	117.5	870	325	1161	this work
QCISD/6-31G*	1.638	116.0	812	330	899	this work
QCISD/6-311G(2d)	1.603	116.1	866	350	968	this work
QCISD/6-311+G(3df)	1.584	115.6	928	369	1029	this work
CCSD(T)/TZ2P	1.619	115.8	822	332	910	20
CCSD(T)/6-311G(2df)	1.607	115.6	⋯	⋯	⋯	20
CCSD(T)/6-311+G(3df)	1.605	115.5	862	350	955	this work
IFCA expt.	1.6135	117.5	820			this work

It can be seen that the computed values are fairly sensitive to the level of calculation employed. The computed minimum energy geometries, harmonic vibrational frequencies, and force constants are required for the subsequent Franck–Condon calculations and spectral simulations. In this connection, the QCISD/6-311G(2d) level of calculation, [see Tables III and IV] appears to be the most appropriate for this purpose, as for the neutral ground state, where experimental values are available, the computed geometrical parameters and harmonic vibrational frequencies obtained at this level of theory match best, of all the calculated results of this work.

The AIE and VIE for the $BrO_2^+(\tilde{X}\,^1A_1)$, $\leftarrow BrO_2(\tilde{X}\,^2B_1)$ ionization were computed at various levels of theory, the highest being the RCCSD(T)/cc-pVQZ level, at different geometries [Table V]. The RCCSD(T)/cc-pVQZ//QCISD/6-311(2d) AIE is identical to the CCSD(T)/6-311+G(3df)//CCSD(T)/6-311(2df) AIE of Francisco[20] of 10.16 eV, suggesting that this value is close to the computational limit (level of correlation and basis set size). The RCCSD(T)/cc-pVQZ VIE obtained using the experimental geometry of the neutral ground state is 10.24 eV, which agrees very well with the experimental VIE (which is equal to the AIE) of 10.26 eV. Inspecting the computed values for BrO_2 and BrO_2^+ [Tables III to V], it seems that it is the computed minimum energy geometries for both the neutral and cationic ground state which require a higher level of calculation. This is also reflected in the best IFCA geometry derived for the cationic ground state and this will be discussed in Sec. IV D 3.

Calculations have also been carried out on the lowest triplet state of BrO_2^+ in order to confirm that the lowest singlet state is the ground cationic state and to assist the search for higher bands of BrO_2. The results are shown in Tables VI and VII. The optimized geometry of the $\tilde{a}\,^3B_2$ state seems to be reasonably stable with respect to the levels of calculation used and corresponds to a large change in both the Br–O bond length and the OBrO bond angle on ionization to this state; this would give rise to a broad photoelectron band showing structure in both the symmetric stretching and bending modes. It is expected that of the levels of calculation used to compute frequencies the QCISD/6-31G* harmonic frequencies are the most reliable [Table VI], with the highest stretching frequency computed to be $\approx$700 cm^{-1}. From Table VII, it can be seen that the computed AIE and VIE values are very sensitive to the levels of calculation used. Nevertheless, at the highest levels of calculation used [G2 and RCCSD(T)/cc-pVQZ], the AIE and VIE to this triplet state are computed to be 11.59 and 11.71 eV, respectively. Therefore, the photoelectron band corresponding to ionization to the lowest triplet state of the cation would be expected to be $\approx$1.2 eV higher than the ionization energy to the lowest singlet state. This can be compared with ClO_2, where the $^3B_2$ state of ClO_2^+ is $\approx$2 eV higher than the $\tilde{X}\,^1A_1$ state.

3. Spectral simulation of the $BrO_2^+\,\tilde{X}^1A_1 \leftarrow BrO_2\,\tilde{X}^2B_1$ ionization

The simulated spectrum obtained using the QCISD/6-311G(2d) geometries and force constants are shown in Fig. 8(a). It can be seen that the main vibrational progression, corresponding to the two components observed experimentally, arises due to excitation of the symmetric stretching mode in the cation, with very weak relative intensities of vibrational components corresponding to excitation of the symmetric bending mode. This is because the computed change in bond angle upon ionization is small [1.3° at the QCISD/6-311G(2d) level]. It is of interest to note that the strongest vibrational component is the (0, 0, 0)-(0, 0, 0) ionization and the AIE coincides with the VIE. This vibrational pattern is significantly different from that of the first band in the HeI photoelectron spectrum of ClO_2, where the most intense component is the second vibrational component. However, the computed BrO_2 envelope matches reasonably well that of the 10.26 eV band observed in the $O+Br_2$ photoelectron spectrum.

Employing the experimental geometry of $r_e = 1.644$ Å and $\theta_e = 114.3$ (from Ref. 38) for $BrO_2(\tilde{X}\,^2B_1)$, the IFCA procedure was performed by varying the cationic geometry to obtain the simulated spectrum which matches best with the experimental HeI photoelectron spectrum. The best simulated spectrum is shown in Fig. 8(b). An estimated experimental resolution (full width half maximum) of 65 meV was used with a Gaussian line shape in this simulation. The IFCA geometry used for the cationic state to produce Fig. 8(b) is $r_e = 1.6135$ Å and $\theta_e = 117.5°$. Although the vibrational components due to excitation of the bending mode were not resolved in the experimental spectrum, the simulations suggested that the slightly asymmetric band shape observed in the HeI photoelectron spectrum [on the high ionization energy (I.E.) side; see Fig. 6(d)] almost certainly arises from contributions from excitation of the bending mode, and the bond angle change on ionization was obtained by matching the asymmetry of the first two observed vibrational bands. The uncertainties in the IFCA derived ionic bond length and

TABLE V. Computed adiabatic and vertical ionization energies of $BrO_2(\tilde{X}\,^2B_1)$ [$BrO_2^+(\tilde{X}\,^1A_1) \leftarrow BrO_2(\tilde{X}\,^2B_1)$].

Method	AIE	VIE	Ref.
MP2/6-31G*	9.29		this work
QCISD/6-31G*	9.98		this work
QCISD/6-311+G(2*d*)	10.11		this work
QCISD/6-311+G(3*df*)	10.39		this work
CCSD(T)/6-311+G(3*df*)	10.16		this work
G2	10.33		this work
RCCSD(T)/cc-pVQZ// QCISD/6-311G(2*d*)	10.16		this work
CCSD(T)/6-311++G(3*df*)// CCSD(T)/6-311G(2*df*)	10.16		20
RCCSD(T)/cc-pVQZ//expt. geom.	···	10.24	this work
Expt.	10.26	10.26	this work

bond angle, based simply on the matching between the simulated and observed spectra are ±0.0010 Å and ±1.0°, respectively. The rather large uncertainty in the bond angle is due to the unresolved bending mode contributions in the experimental spectrum. However, because of experimental uncertainties in the relative component intensities and the uncertainty in the experimental r_e for the neutral state, the errors in r_e and θ_e in the ionic state are estimated as ±0.005 Å and ±2.0°, respectively. Comparison between the *ab initio* computed geometrical parameters and the experimentally derived values suggests that there is an overestimate in the decrease in the bond length and an underestimate of the increase in bond angle upon ionization in the theoretical values.

4. Ab initio calculations of vibrational frequencies and ionization energies of Br_2O

As already stated, the band at 10.26 eV observed in the $O+Br_2$ reaction can be unambiguously assigned to ionization of $BrO_2(C_{2v})$. However, computed results obtained for different isomers of Br_2O will now be presented to show that these cannot be assigned to the 10.26 eV band. The computed positions and envelopes may well be of use in identifying products of future experiments.

Calculations were performed on

(a) C_{2v} BrOBr and C_s BrBrO singlet states, with ionization to the lowest doublet ionic states. Singlet BrOBr (C_{2v}) is known to be lower than singlet BrBrO by ≈0.7 eV.[39]

TABLE VI. $BrO_2^+\,\tilde{a}\,^3B_2$ calculated optimized geometries and harmonic vibrational frequencies.[a]

Method Parameter	HF/6-31G*	MP2/6-31G*	QCISD/6-31G*
OBr/A	1.733	1.728	1.757
OBrO/deg	101.5	104.4	104.7
Sym.str/cm^{-1}	685	849	695
Sym.bend/cm^{-1}	312	297	271
Asym.str./cm^{-1}	666	722	537

[a]The dominant configuration of $BrO_2^+(\tilde{a}\,^3B_2)$ is $\text{- - - } a_2^1\, b_1^1$.

TABLE VII. Computed $BrO_2^+(\tilde{a}\,^3B_2) \leftarrow BrO_2(\tilde{X}\,^2B_1)$ ionization energies/eV.

Method	AIE	VIE	Ref.
MP2/6-31G*	11.57		this work
MP2/6-311+G(3*df*)//MP2/6-31G*	12.37		this work, G2
MP4/6-311G*//MP2/6-31G*	11.22		this work, G2
MP4/6-311+G*//MP2/6-31G*	11.55		this work, G2
MP4/6-311G(2*d*,*f*)//MP2/6-31G*	11.71		this work, G2
G2	11.59		this work
QCISD/6-31G*	10.47		this work
QCISD(T)/6-311G*//MP2/6-31G*	10.70		this work, G2
RCCSD(T)/cc-pVQZ//QCISD/6-31G*, 6-311G(2*d*)	11.56		this work
RCCSD(T)/cc-pVQZ//expt		11.71	this work

(b) Triplet BrBrO and triplet BrOBr states, with ionization to the lowest doublet and quartet ionic states. These calculations were performed because the $O(^3P) + Br_2(X\,^1\Sigma_g^+)$ reaction is expected to proceed on a triplet surface and may yield triplet Br_2O as the final product. These open-shell triplet states lie higher in energy than the corresponding closed-shell singlet states.

In all cases the computed envelopes did not match that of the envelope of the band seen at 10.26 eV from the $O+Br_2$ reaction. Hence, only the results of the C_{2v} BrOBr and C_s BrBrO calculations will be presented here.

The optimized geometries and harmonic vibrational frequencies of both structures of Br_2O have been computed by Lee,[40] employing the CCSD(T)/TZ2P level of calculation. More recently, Kolm *et al.*[39] reported a combined matrix isolation infrared spectroscopy and *ab initio* study on the photoinitiated isomerization between these two structures. In both studies, the BrOBr structure was found to be lower in energy and the ground electronic states of both structures are closed-shell singlet states. Also, in Ref. 39, the vertical excitation energies from the closed-shell ground state of both structures to their low-lying singlet and triplet states were computed by the MCQDPT2 method. To our knowledge, no *ab initio* calculations have been performed on the cationic states of BrOBr or BrBrO. Since the BrOBr is the more stable, it may be expected that BrOBr would be the product when Br_2O is produced. However, BrBrO has a computed harmonic vibrational frequency of 793 cm^{-1} for the BrO stretch,[40] which is close to the vibrational separation observed for the 10.26 eV band observed from the $O+Br_2$ reaction, whereas the vibrational frequencies of BrOBr are all lower [the symmetric stretching mode in BrOBr is 525 cm^{-1}; see Table VIII].

Using the methods adopted in the BrO_2 calculations, minimum energy geometries and harmonic frequencies were computed at several levels of theory with different standard basis sets, for the ground electronic states of both the neutral and cationic states of both structures.

The optimized geometries and harmonic vibrational frequencies computed in this work are summarized in Tables VIII–XI. For BrOBr, the results obtained agree very well with the CCSD(T) values of Lee[40] [see Table VIII], suggesting that in this case both the ECP basis set and the B3LYP

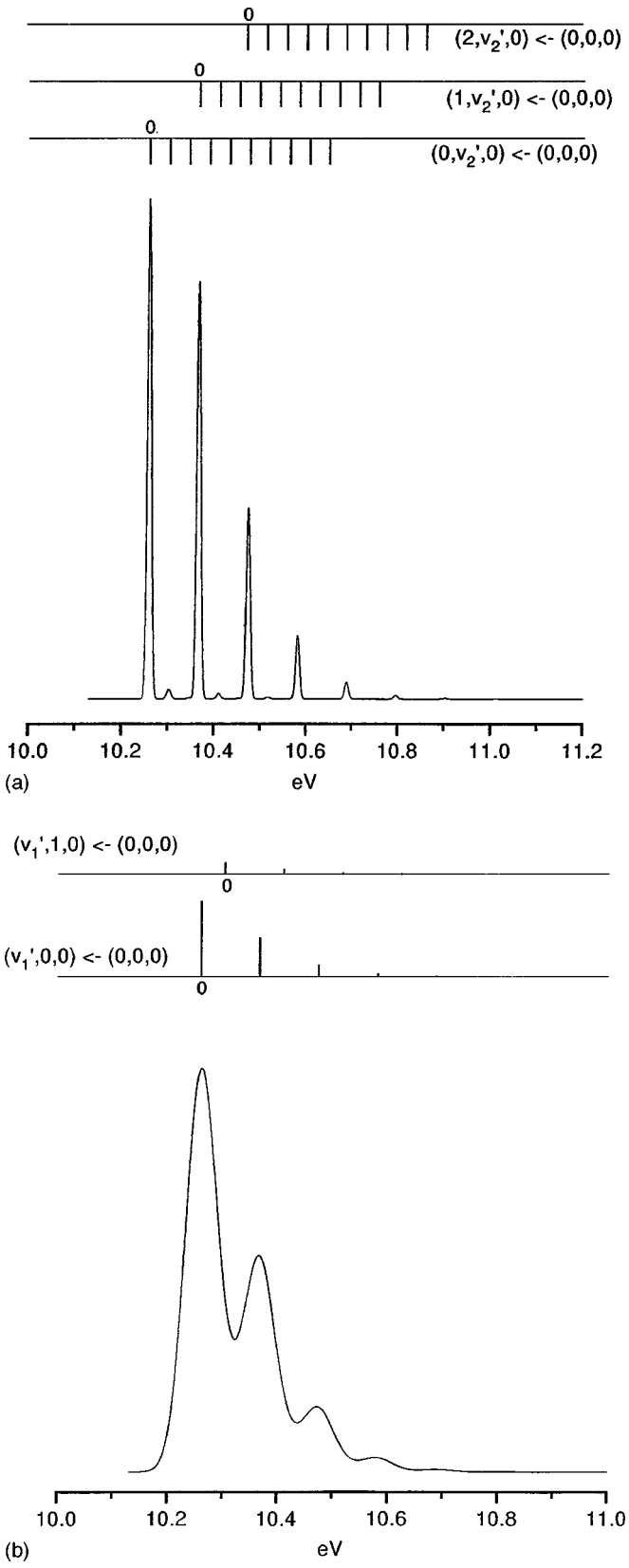

FIG. 8. (a) Simulation of the first BrO_2 band using results of QCISD/6-311G($2d$) calculations. Gaussian vibrational envelopes with a FWHM of 10 meV were used in this simulation (see text for further details). (b) Simulation of the first band of BrO_2 using the IFCA procedure and the experimental equilibrium geometry of Ref. 38. Gaussian vibrational envelopes with a FWHM of 65 meV were used in this simulation (see text for further details).

TABLE VIII. Optimized geometries and harmonic vibrational frequencies of the $\tilde{X}\,^1A_1$ state of BrOBr(C_{2v}).

Method	BrO/Å	θ/°	$v_1(a_1)$	$v_2(a_1)$	$v_3(b_2)$
MP2/lan12$dz+2d$[a]	1.880	111.7	516	181	647
B3LYP/lan12$dz+2d$[a]	1.873	114.5	526	178	598
B3LYP/6-311G($3df$)	1.854	114.7	535	183	616
QCISD/lan12$dz+2d$	1.869	113.3	535	181	664
CCSD(T)/TZ2P[b]	1.865	112.9	513	180	613
Microwave[c]	1.83786	112.249			
IR Ar[d]			525.3		622.2

[a]The 6-31+G($2d$) basis set was used for O; see text.
[b]Reference 40.
[c]Reference 11.
[d]Reference 39.

method used are reasonable alternatives for the more demanding all-electron basis sets and traditional correlation methods, respectively. When comparing with the available experimental values for BrOBr ($\tilde{X}\,^1A_1$) [Table VIII] and BrBrO ($\tilde{X}\,^1A'$) [Table X], agreement is good except for the BrO bond length of BrOBr, where the computed values are consistently too large. For BrBrO, and the ground cationic states of both structures, the demand on theory seems to be higher, as the computed results vary with different levels of calculation. In particular, the MP2 level seems inadequate for the $\tilde{X}\,^2B_1$ state of $BrOBr^+$, where the v_3 mode has an imaginary value.

In relation to the assignment of the 10.26 eV photoelectron band in the $O+Br_2$ reaction, the computed vibrational frequencies of the ground cationic states of the two structures are particularly relevant, as no experimental values are available. From Tables IX and XI, it was concluded that the QCISD values should be reasonably reliable. Based on these computed vibrational frequencies, the energetically less stable BrBrO structure is favored for the assignment of the 10.26 eV photoelectron band over BrOBr, as for $BrBrO^+$, the BrO stretching mode has a calculated harmonic frequency of over 700 cm^{-1}, while all the calculated vibrational frequencies of $BrOBr^+$ are significantly less than the observed vibrational spacing of 820 cm^{-1}.

In Table XII, the computed first AIEs of both structures are summarized. For BrOBr, we have also computed the first AIE at the RCCSD(T)/cc-pVQZ level, with the QCISD/6-331+G($2d$) and experimental geometries for the cation [Table IX] and neutral [Table VIII], respectively. At this level of calculation, an AIE of 10.37 eV was obtained, which can be compared with the first AIE of 10.34 eV, obtained at a similar level of theory for BrO [RCCSD(T)/cc-pVQZ at CASSCF/MRCI geometries]. A very similar comparison can be obtained when the results at the G2 level of calculation are also considered (for BrO, a G2 first AIE value of 10.37 eV was reported in Ref. 8). Therefore, based on the computed AIEs, the first bands of BrOBr and BrO would be expected to coincide, while that of BrBrO is $\approx$0.44 eV lower in energy (at the G2 level, see Table XII). With the measured first AIE of 10.46 eV for BrO from PES, these values lead to

TABLE IX. Calculated optimized geometries and harmonic vibrational frequencies of the $\tilde{X}\,^2B_1$ state of $BrOBr^+$ (C_{2v}).

Method	BrO/Å	θ/°	$\nu_1(a_1)$	$\nu_2(a_1)$	$\nu_3(b_2)$
UHF/6-31G*	1.807	122.1	443	177	514
CASSCF(5,5)/lan12dz+2d	1.887	116.5	422	166	566
MP2/6-31G*	1.740	120.8	785	244	846i[c]
MP2/lan12dz+2d[a]	1.738	121.1	793	240	1005i[c]
B3LYP/6-31G*	1.816	120.4	542	203	639
B3LYP/lan12dz+2d[a]	1.814	121.2	548	198	622
B3LYP/6-311G(3df)	1.797	121.7	546	200	639
QCISD/lan12dz+2d	1.823	119.7	538	192	545
QCISD/6-31G*[b]	1.835	119.3	535	191	555
QCISD/6-311G(2d)	1.812	119.6	535	194	542

[a]The 6-31+G(2d) basis set was used for O; see text.
[b]The five components d Gaussian functions were used instead of the default size components.
[c]The ''i'' indicates an imaginary frequency.

an expected AIE of 10.02 eV for BrBrO, while the measured value from the $O+Br_2$ photoelectron spectrum is 10.26 eV.

In view of these considerations of the AIE positions, the assignment of the 10.26 eV band to either C_{2v}BrOBr or C_sBrBrO cannot be made—one is expected to be ≈0.15 eV higher while the other is ≈0.29 eV lower than the observed value. Although in the case of BrO, it has been demonstrated[7] that extrapolation of CCSD(T) calculations to the basis set limit gave the best theoretical estimate of the AIE, which agreed with the experimental value to within ±0.02 eV, such an extrapolation to the basis set limit for Br_2O is beyond our present computational capacity.

5. Spectral simulations for Br_2O–C_{2v} BrOBr and C_s BrBrO

Spectral simulations were carried out employing the QCISD values, obtained with the largest basis sets used (see Tables VIII–XI) for both BrOBr and BrBrO. The simulated spectra for the C_{2v} and the C_s structures are shown in Figs. 9 and 10. It can be seen that the simulated vibrational envelopes for the first bands of both BrOBr and BrBrO are much more complex than the rather simple observed band envelope of the 10.26 eV band of a single progression showing only two vibrational components [Fig. 6(d)]. The simulations show that structure in more than one vibrational mode is observed in the first photoelectron bands of BrOBr and BrBrO, in accordance with the computed changes in equilibrium geometry upon ionization (Tables VIII–XI). Based on these simulations, it is clear that the first photoelectron bands of BrOBr and BrBrO would not have a simple band envelope, as is observed for the band at 10.26 eV in the $O+Br_2$ reaction. This photoelectron band cannot therefore be assigned to ionization of C_{2v} BrOBr or C_s BrBrO.

TABLE X. Calculated optimized geometries and harmonic vibrational frequencies of the $\tilde{X}\,^1A$ state of BrBrO(C_s).

Method	BrO/Å	BrBr/Å	θ/Å	ν_1 (BrO)	ν_2 (BrBr)	ν_3 (bend)
HF/6-31G*	1.691	2.315	108.4	669	332	194
CASSCF(8,7)/6-31G*	1.711	2.548	113.3	774	131	179
MP2/6-31+G*	1.659	2.466	113.85	1035	238	170
MP2/lan12dz+2d[a]	1.656	2.525	113.9	1030	228	160
B3LYP/lan12dz+2d[a]	1.687	2.489	112.4	801	240	166
B3LYP/6-311G(3df)	1.669	2.434	111.9	844	253	175
QCISD/lan12dz+2d	1.710	2.483	110.4	719	246	161
QCISD/6-311G(2d)	1.693	2.470	111.6	737	247	165
CCSD(I)/TZ2P[b]	1.690	2.510	113.1	793	215	153
IR (Ar)[c]				804	235.8	
IR (Ar)[d]				804.6		

[a]The 6-31+G(2d) basis set was used for O; see text.
[b]Reference 40.
[c]Reference 44.
[d]Reference 39.

TABLE XI. Calculated optimized geometries and harmonic vibrational frequencies of the $\tilde{X}\,^2A'$ state of $BrBrO^+$ (C_s).

Method	BrO/Å	BrBR/Å	θ/°	ν_1 (BrO)	ν_2 (BrBr)	ν_3 (bend)
UHF/6-31G*	1.740	2.281	102.8	632	332	214
CASSCF(7,7)/6-31G*	1.700	2.288	106.5	693	326	209
CASSCF(7,7)lan12dz+2d[a]	1.784	2.398	101.7	536	274	176
MP2(full)/6-31G*	1.701	2.288	106.1			
MP2/lan12dz+2d[a]	1.678	2.239	106.8	700	300	200
B3LYP lan12dz+2d[a]	1.662	2.357	110.5	779	281	195
B3LYP/6-311G(3df)	1.651	2.300	109.9	806	204	206
QCISD/lan12dz+2d	1.687	2.368	108.3	729	275	188
QCISD/6-311G(2d)	1.677	2.342	108.6	738	286	194

[a]The 6-31+G(2d) basis set was used for O; see text.

6. Triplet BrO.Br and OBr.Br, and their cationic states

A large number of low-lying open-shell triplet neutral and quartet/doublet cationic states were investigated. Most of them were found to have one short and one long bond (>3.0 Å) for both the neutral and cation. To achieve spectral assignment, only the lowest states are considered here.

Geometry optimization of the lowest triplet state of BrO.Br at the MP2/6-31+G* and QCISD/6-31G* levels led to both bent (C_s) and linear ($C_{\infty v}$) structures. The lowest energy minima are $^3A''$ and $^3\Pi$, which are very close in energy with the $^3A''$ state lower than the $^3\Pi$ state. These states are almost certainly part of the same triplet surface. Both minimum energy structures have short (≈1.77 Å) and long (≈2.70 Å) Br–O bonds. Spectral simulations performed for the ionizations $BrO^+.Br(^4A', ^4A'') \leftarrow BrO.Br(^3A'')$ gave in each case a Franck–Condon envelope consisting of one broad band with vibrational structure in ν_2'(≈210 cm^{-1}) and

TABLE XII. Computed first adiabatic ionization energies (in eV) for BrOBr and BrBrO.

Method	$\tilde{X}\,^2B_1$ $BrOBr^+$	$\tilde{X}^2A''BrBrO^+$
HP/6-31G*	9.80	8.20
MP2(full)/6-31G*	10.41	9.75
MP2/lan12dz+2d[a]	10.48	10.20
B3LYP/lan12dz+2d[a]	10.01	9.78
B3LYP/6-311G(3df)	9.97	9.59
QCISD/lan12dz+2d[a]	10.07	9.57
QCISD/6-311G(2d)	⋯	9.42
G2	10.37	9.93

[a]The 6-31+G(2d) basis set was used for O; see text.

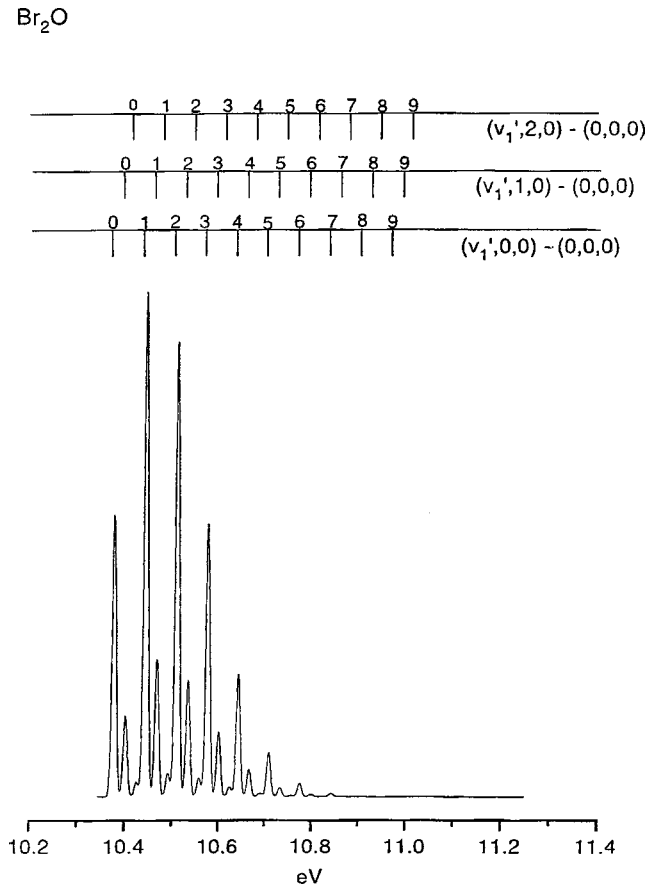

FIG. 9. Simulated first photoelectron band of C_{2v} BrOBr using QCISD computed values for the neutral and ionic states involved. Gaussian vibrational envelopes with a FWHM of 10 meV were used in this simulation (see text for further details).

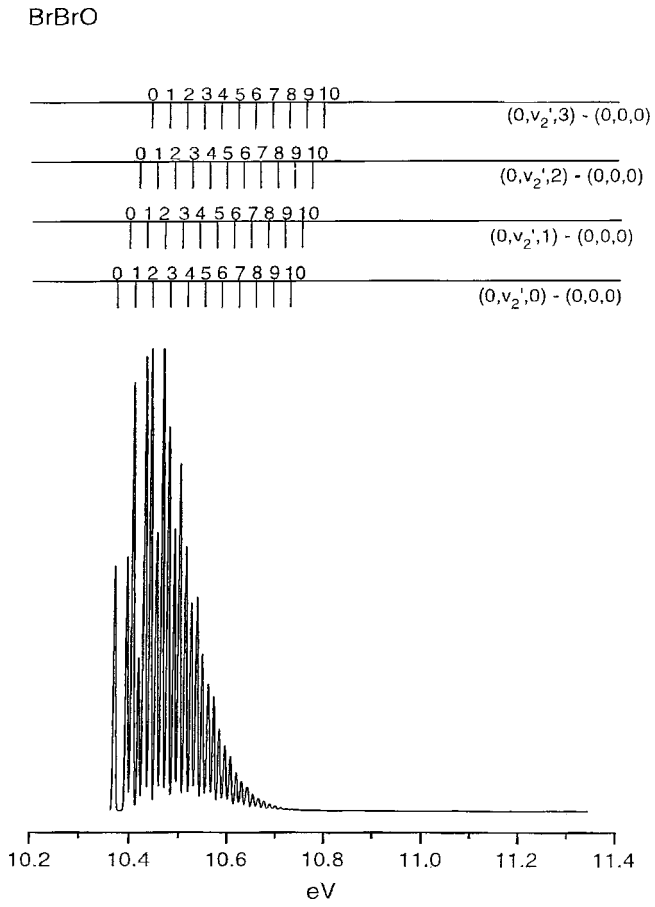

FIG. 10. Simulated first photoelectron band of C_s BrBrO using QCISD computed values for the neutral and ionic states involved. Gaussian vibrational envelopes with a FWHM of 5 meV were used in this simulation (see text for further details).

v_3' ($\approx 76\,cm^{-1}$), showing very poor agreement with the envelope of the band at 10.26 eV seen in the $O+Br_2$ reaction.

Similar results were obtained for OBr.Br. At the QCISD/6-31+G* level, the lowest energy state is $^3\Sigma^-$, with a $^3A''$ state slightly higher in energy, and the lowest energy ionization is expected to be $OBr^+.Br(\tilde{X}\,^4\Pi) \leftarrow OBr.Br(\tilde{X}\,^3\Sigma^-)$. One highly structured broad band is computed for this ionization, consisting of overlapped series in the Br–Br stretching mode ($v_2' \approx 95\,cm^{-1}$) for excitation to $v=0$, 1, 2, and 3 in the Br–O stretching mode ($v_1' \approx 740\,cm^{-1}$). Again, very poor agreement was obtained with the envelope of the 10.26 eV band observed from the $O+Br_2$ reaction.

The conclusion from all these simulations is that the 10.26 eV band observed in the $O+Br_2$ reaction system is the first photoelectron band of BrO_2.

Although BrO_2 is clearly produced, its production mechanism is not well established. There have been two suggestions in the literature.[21,41] The first involves the reaction sequence.[41]

$$O+Br_2 \rightarrow BrO+Br, \tag{5}$$

$$O+BrO+M \rightarrow BrO_2+M, \tag{6}$$

$$O+BrO \rightarrow Br+O_2. \tag{7}$$

The rapid reaction (7) competes with reaction (6), and Br atoms were observed in this work as a secondary product of the $O+Br_2$ reaction.

More recently it has been proposed[21] that BrO_2 is produced by reaction of vibrationally excited $BrO(BrO^\dagger)$ with itself or with thermalized BrO, i.e.,

$$BrO^\dagger+BrO^\dagger \rightarrow BrO_2+Br, \tag{8}$$

$$BrO^\dagger+BrO \rightarrow BrO_2+Br. \tag{9}$$

In our experiments, although BrO_2 was clearly seen in the $O+Br_2$ reaction, it was not observed in the $Br+O_3$ reaction even when BrO was clearly present. These observations may be explained by noting that ground-state BrO_2 reacts with ozone very slowly but vibrationally excited BrO_2 is at least three orders of magnitude more reactive toward ozone than ground-state BrO_2. If BrO_2 is produced via reactions (8) or (9) in the $Br+O_3$ reaction mixture, its partial pressure is kept low because BrO_2 is produced vibrationally excited and is removed by reaction with ozone. We feel, therefore, that as proposed in Ref. 21, reactions (8) and (9) represent the most likely reactions for BrO_2 production in the $O+Br_2$ reaction sequence.

V. CONCLUSIONS

The main conclusion of this work is that the photoelectron band associated with a reaction product of the $O+Br_2$ reaction in the early PES work,[17] and initially assigned to BrO, is actually associated with ionization of the secondary reaction product BrO_2. This band at (10.26 ± 0.02) eV ionization energy can be firmly assigned as the $BrO_2^+(\tilde{X}\,^1A_1) \leftarrow BrO_2(\tilde{X}\,^2B_1)$ ionization on the basis of computed AIEs and Franck–Condon simulations performed in this work. The first photoelectron band of BrO, prepared from reaction (1), is vibrationally resolved and allows the first AIE of BrO to be measured as (10.46 ± 0.02) eV, in good agreement with previous measurements from photoionization mass spectrometry.[18] Assuming $BrO(X\,^2\Pi)$ dissociates to $Br(^2P)$ and $O(^3P)$ and $BrO^+(X\,^3\Sigma)$ dissociates to $Br^+(^3P)$ and $O(^3P)$, then $D_0^0(BrO)$ of (2.39 ± 0.03) eV[42] and the first ionization energy of atomic bromine of 11.81 eV[24,29] can be combined with the first ionization energy of BrO of (10.46 ± 0.02) eV measured in this work to yield $D_0^0(BrO^+, X\,^3\Sigma^-)$ of (3.74 ± 0.05) eV.

ACKNOWLEDGMENTS

The authors thank EPSRC, the Leverhulme Trust, and the Research Grant Council of Hong Kong for financial support of this work (Grant Nos. PolyU 5156/98P and PolyU 5180/99P).

[1] D. J. Lary, J. Geophys. Res. **101**, 1505 (1996).
[2] D. J. Lary, J. Geophys. Res. **102**, 21515 (1997).
[3] U. Platt and C. Janssen, Faraday Discuss. **100**, 175 (1995).
[4] E. A. Cohen, H. M. Pickett, and M. Geller, J. Mol. Spectrosc. **87**, 459 (1981).
[5] J. E. Butler, K. Kawaguchi, and E. Hirota, J. Mol. Spectrosc. **104**, 372 (1984).
[6] M. D. Wheeler, S. M. Newman, T. Ishiwata, M. Kawasaki, and A. J. Orr-Ewing, Chem. Phys. Lett. **285**, 346 (1998).
[7] J. S. Francisco, S. Parthiban, and T. J. Lee, J. Chem. Phys. **109**, 10818 (1998).
[8] N. L. Ma, Y. S. Cheung, C. Y. Ng, and W. K. Li, Mol. Phys. **91**, 495 (1997).
[9] D. Papayannis, A. M. Kosmas, and V. S. Melissas, Chem. Phys. Lett. **243**, 249 (1999).
[10] H. S. P. Müller, C. E. Miller, and E. A. Cohen, Angew. Chem. Int. Ed. Engl. **35**, 2129 (1996).
[11] H. S. P. Müller and E. A. Cohen, J. Chem. Phys. **106**, 8344 (1997).
[12] M. P. McGrath and F. S. Rowland, J. Phys. Chem. **100**, 4815 (1996).
[13] L. F. Pacios and P. C. Gómez, J. Phys. Chem. A **101**, 1767 (1997).
[14] M. A. Workman and J. S. Francisco, Chem. Phys. Lett. **293**, 65 (1998).
[15] M. Alcami and I. L. Cooper, J. Chem. Phys. **108**, 9414 (1998).
[16] M. Alcami, O. Mó, M. Yanex, and I. L. Cooper, J. Phys. Chem. A **103**, 2793 (1999).
[17] S. J. Dunlavey, J. M. Dyke, and A. Morris, Chem. Phys. Lett. **53**, 382 (1978).
[18] P. S. Monks, L. J. Stief, M. Krauss, S. C. Kuo, and R. B. Klemm, Chem. Phys. Lett. **211**, 416 (1993).
[19] R. P. Thorn, P. S. Monks, L. J. Stief, S. C. Kuo, Z. Zhang, and R. B. Klemm, J. Phys. Chem. **100**, 12199 (1996).
[20] J. S. Francisco, Chem. Phys. Lett. **288**, 307 (1998).
[21] Z. Li, J. Phys. Chem. A **103**, 1206 (1999).
[22] J. M. Dyke, A. Morris, and N. Jonathan, Int. Rev. Phys. Chem. **2**, 3 (1982).
[23] R. P. Wayne, Atmos. Environ. **29**, 2677 (1995).
[24] D. Wang, C. Li, X. Qian, and S. D. Gamblin, J. Electron Spectrosc. Relat. Phenom. **97**, 59 (1998).
[25] J. M. Dyke, L. Golob, N. Jonathan, and A. Morris, J. Chem. Soc., Faraday Trans. 2 **70**, 1828 (1974).
[26] GAUSSIAN 94, Revision E3, M. J. Frisch, G. W. Trucks, H. B. Schlegel, P. M. W. Gill, B. G. Johnson, M. A. Robb, J. R. Cheeseman, T. Keith, G. A. Peterson, J. A. Montgomery, K. Raghavachari, M. A. Al-Laham, V. G. Zakrzewski, J. V. Ortiz, J. B. Foresman, J. Cioslowski, B. B. Stefanov, A. Nanayakkara, M. Challacombe, C. Y. Peng, P. Y. Ayala, W. Chen, M. W. Wong, J. L. Andres, E. S. Replogle, R. Gomperts, R. L. Martin, D. J. Fox, J. S. Binkley, D. J. Defrees, J. Baker, J. P. Stewart, M. Head-Gordon, C. Gonzalez, and J. A. Pople, Gaussian Inc., Pittsburgh, PA, 1995.
[27] MOLPRO 96.4, H. J. Werner and P. J. Knowles, with contributions from J. Almlöf, R. D. Amos, A. Berning, M. J. O. Deegan, F. Eckert, S. T. Elbert, C. Hampel, R. Lindh, W. Meyer, A. Nicklass, K. Peterson, R. Pitzer, A. J. Stone, P. R. Taylor, M. E. Mura, P. Pulay, M. Schuetz, H. Stoll, T. Thorsteinsson, and D. L. Cooper.
[28] J. C. Green, M. L. H. Green, P. J. Joachim, A. F. Orchard, and D. W. Turner, Philos. Trans. R. Soc. London, Ser. A **268**, 111 (1970).
[29] C. E. Moore, Atomic Energy Levels, Circular No. 467, N.B.S., U.S. Dept. of Commerce, Washington D. C. (U.S. Govt. Printing Office 1952), Vol. II.
[30] T. Amano, A. Yoshinagu, and E. Hirota, J. Mol. Spectrosc. **44**, 594 (1972).
[31] J. M. Dyke, J. Chem. Soc., Faraday Trans. 2 **83**, 67 (1987).
[32] R. J. Le Roy, Chemical Physics Research Report (CP330), University of Waterloo, 1991.
[33] F. T. Chau, J. M. Dyke, E. P. F. Lee, and D. C. Wang, J. Electron Spectrosc. Relat. Phenom. **97**, 33 (1998).
[34] W. R. Wadt and P. J. Hay, J. Chem. Phys. **82**, 284 (1985).
[35] E. P. F. Lee and T. G. Wright, J. Phys. Chem. A **101**, 1374 (1997).
[36] L. A. Curtiss, K. Raghavachari, G. W. Trucks, and J. A. Pople, J. Chem. Phys. **94**, 7221 (1991).
[37] K. A. Peterson and H. J. Werner, J. Chem. Phys. **99**, 302 (1993), and Ref. 7 therein; R. Flesch, E. Rühl, K. Hottmann, and H. Baumgartel, J. Phys. Chem. **97**, 837 (1993).
[38] H. S. P. Muller, C. E. Miller, and E. A. Cohen, J. Chem. Phys. **107**, 8292 (1997).
[39] J. Kolm, O. Schrems, and P. Beichart, J. Phys. Chem. A **102**, 1083 (1998).
[40] T. J. Lee, J. Phys. Chem. **90**, 15074 (1995).
[41] N. I. Butkovskaya, I. I. Morozov, V. L. Talrose, and E. S. Vasiliev, Chem. Phys. **79**, 21 (1983).
[42] R. A. Durie and D. A. Ramsey, Can. J. Phys. **36**, 35 (1958).
[43] K. A. Peterson, J. Chem. Phys. **109**, 8864 (1998).
[44] D. Tevault, N. Walker, R. R. Smardzewski, and W. B. Fox, J. Phys. Chem. **82**, 2733 (1978).